ACS APPLIED MATERIALS & INTERFACES

www.acsami.org

Research Article

Unidirectional Transport and Effective Collection of Underwater CO_2 Bubbles Utilizing Ultrafast-Laser-Ablated Janus Foam

Suwan Zhu, Jiawen Li,* Shengwen Cai, Yucheng Bian, Chao Chen, Bing Xu, Yahui Su, Yanlei Hu, Dong Wu,* and Jiaru Chu

Cite This: *ACS Appl. Mater. Interfaces* 2020, 12, 18110−18115

Read Online

ACCESS | Metrics & More | Article Recommendations | Supporting Information

ABSTRACT: Manipulating gas bubbles in aqueous ambient is of great importance for applications in water treatment, gas collection, and matter transport. Here, a kind of Janus foam is designed and fabricated by one-step ultrafast laser ablation of one side of the copper film, which is treated to be superhydrophobic. Janus foam exhibits not only the capability of unidirectional transport of underwater bubbles but also gas collection with favorable efficiency up to ∼15 mL cm^{-2} min^{-1}. The underlying physical mechanism is attributed to the cooperation of the buoyancy, adhesion, and wetting gradient forces imposed on the bubbles. As a paradigm, the underwater chemical reaction between the unidirectional CO_2 gas flow and the alkaline phenolphthalein solution is demonstrated via Janus foam. This facile and low-cost fabrication approach for Janus foam will find broad potential applications in effective bubble transport, carbon capture, and controllable chemical reactions under aqueous conditions.

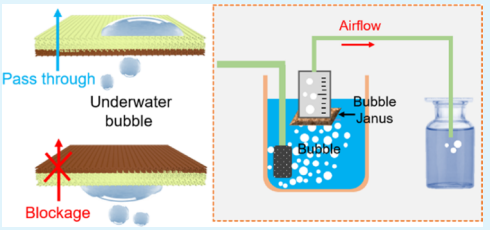

KEYWORDS: *unidirectional bubble transport, directional bubble collection, Janus foam, ultrafast laser, wetting gradient force*

1. INTRODUCTION

Bubbles are ubiquitous in nature and organisms but remain challenging to understand and manipulate. The effective manipulation regarding collection, transport, and the chemical reaction for underwater gas bubbles plays a crucial role in both scientific research and industrial applications such as water treatment, mineral flotation, and microreactions in aqueous ambient.[1−4] For instance, by virtue of an agitation way that creates small bubbles, more surfaces are produced to capture the contaminants by the floating froth and clarify wastewaters. For living creatures, the humpback whales hunt fishes by producing numerous tiny gas bubbles around them.[5] In industrial settings, quick detachment of gas bubbles on a heated surface can significantly boost the efficiency of boiling heat transfer.[6−9] Moreover, capturing and collecting gas bubbles can elevate the gas diffusivity in aqueous ambient, followed by accelerating the mass exchange efficiency in the ocean.[10] Consequently, the realization of directional transport and effective collection of gas bubbles are of vital importance for various potential applications.

In order to manipulate underwater gas bubbles, a variety of microstructures have been developed such as metallic meshes, organic sheets or microcones, and so forth.[11−15] Hu et al. realized a channel-controlled Janus membrane for underwater unidirectional bubble penetration by a femtosecond laser-assisted ablation and nanoparticles deposition approach.[16] Lu et al. developed a superaerophilic carbon-nanotube-array electrode using a solvothermal method, which would boost the oxygen-bubble adhesion and the diffusion process.[17] Jiang and coworkers reported a reliable bubble manipulation sheets via regulating a series of interfaces with well-ordered microstructures and controllable chemical compositions on silicon surfaces.[18] Generally, most of these substrates can be divided into superhydrophobic/superhydrophilic surfaces[12,19−21] and lubricant-infused surfaces.[22−26] Among these, three driving forces can be considered to be the sources of bubble transport: buoyancy,[22,23,27] wetting gradient, and Laplace gradient forces arising from substrate's properties.[12,19,25,26] For buoyancy-based cases, an upward motion of gas bubbles can be realized via dynamically rotating and tilting the substrate.[19,22,23] For wetting gradient and Laplace gradient forces, effective bubble transport can be achieved via surface energy modification and specially designed morphology.[24,28]

As a kind of typical wetting gradient device, Janus membrane, featuring superhydrophobicity and superhydrophilicity on two opposite surfaces, has exhibited excellent capability of unidirectional bubble penetration and demonstrated the potential applications in underwater bubble manipulation.[11,29,30] Nevertheless, current studies on "bubble Janus" mainly focus onto realizing the unidirectional bubble passage/blockage capability (i.e., "bubble diode"). The relevant bubble collection efficiency is rarely mentioned. In a practical scenario, the collection

Received: January 9, 2020
Accepted: March 25, 2020
Published: March 25, 2020

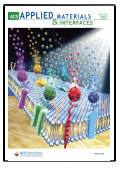

https://dx.doi.org/10.1021/acsami.0c00464
ACS Appl. Mater. Interfaces 2020, 12, 18110−18115

efficiency of bubble Janus is undoubtedly crucial and, therefore, should be further concerned. Metallic foams (e.g., copper and nickel), featuring the advantages of low density, high porosity, and mechanical flexibility, are capable of transporting and collecting water droplets unidirectionally.[31,32] Nevertheless, there are few reports available on underwater bubble manipulation with the use of metallic foams.

Herein, we fabricate a kind of Janus copper foam for unidirectional transport and effective collection of underwater gas bubbles. Janus foam is constructed via one-step laser ablation on a single side of the superhydrophobicity-treated copper foam. This Janus foam exhibits not only the capability of unidirectional penetration of underwater gas bubbles from the laser-treated side to the opposite side but also effective gas collection performance by reaching up to ~15 mL cm^{-2} min^{-1} at a 1 m s^{-1} laser scanning speed. As a demonstration for underwater carbon capture, Janus foam allows the CO_2 gas flow to penetrate the "bubble diode" and react with the alkaline phenolphthalein solution. This bubble Janus with facile fabrication and favorable collection performance will find broad applications in bubble transport, carbon capture, and controllable gaseous reactions.

2. RESULT AND DISCUSSION

We choose copper foam to fabricate the bubble Janus because it has a relatively larger specific surface than that of traditional membrane-shaped Janus. Commercially available copper foam sheets (thickness ~1 mm) were cleaned ultrasonically in acetone. The foam PPI (defined as the pore amount per linear inch) was chosen to be 90, 130, and 160, respectively. The cleaned samples were then treated with chemical coating to exhibit superhydrophobicity. Thereafter, the superhydrophobic copper foams were ablated by line-by-line ultrafast laser scanning on one side to form Janus foams (Figure 1a). The

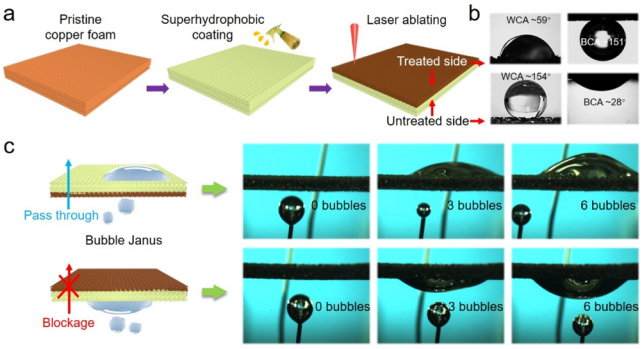

Figure 1. Schematic fabrication of Janus foam and its unidirectional penetration behavior of underwater gas bubbles. (a) Janus foam is fabricated via superhydrophobic coating followed by laser ablation on copper foam. (b) WCA and BCA of 5 μL water droplet and gas bubble on laser-treated and -untreated sides of the Janus foam, respectively. (c) Spontaneous and unidirectional penetration of gas bubbles from laser-treated side to untreated sides of the Janus foam.

laser fabrication system and optical path can be found in our previous work.[20] After the single-side laser ablation, the laser-treated side of copper foam turned dark, showing hydrophilicity with a water contact angle (WCA) of 59° and superaerophobicity with a bubble contact angle (BCA) of 151°, respectively. Whereas the untreated side (i.e., the superhydrophobic side) maintained pristine purple-red, on which WCA and BCA were measured to be 154 and 28°, respectively (Figure 1b). It is observed that Janus foam allows gas bubble to penetrate from laser-treated side to the other side but not in the opposite direction (Figure 1c, Movie S1). Our Janus foam exhibits an excellent unidirectional bubble transport property.

The surface morphology and chemical element analysis of pristine, superhydrophobic, and laser-treated copper foams are further characterized. As shown in Figure 2a (top row), a cellular-like structure was observed on the surface of pristine foam. Judging from the magnified scanning electron microscopy (SEM) image (middle row), the surface of a single copper branch was relatively smooth. Energy-dispersive X-ray spectroscopy (EDS, bottom row) revealed that the proportions (atom %) of elements Cu, O, and Si were 99.54, 0.44, and 0.02%, respectively, which illustrates that the primary element was pristine copper. For the superhydrophobic copper foam (Figure 2b), the magnified SEM image shows that the roughness of the copper branch was elevated because of the existence of superficial Glaco coating which contained superhydrophobic silica nanoparticles. As a consequence, the proportions of elements O and Si were significantly increased by up to 21.56 and 8.89%, respectively, while the proportion of Cu correspondingly decreased to 69.55%. It should be noted that the laser-treated superhydrophobic foam exhibited micro/nanoscale composite structures (Figure 2c). During the laser ablation process, the initial frame of copper foam remained unchanged, but the smooth surface of each branch was induced by a femtosecond laser to generate hollow porous microstructures under the combined effect of laser shock compression and debris deposition. The average size of the hollow pore was estimated to be 4 μm, as shown in Figure 2c. More details can be found in the magnified SEM image in which the flat branch surface was interspersed with sporadic micro- and nano-mastoids because of high energy laser ablation.[33,34] In essence, the formation of nano-mastoids was attributed to the resultant of plasma expansion, local burst, and recrystallization of the irradiated matter. As compared with that of the superhydrophobic foam, O and Si components of the laser-ablated sample had diminished (2.81 and 0.19%, respectively), which were still slightly greater than that of the pristine one.

Realizing effective gas/bubble collection is important for bubble Janus designs in an aqueous environment. Till date, existing studies on bubble Janus mainly focus onto realizing the passage/blockage capability with regard to bubbles, whereas the related collection efficiency is rarely mentioned. To investigate bubble collection efficiency of our Janus foam, we setup a purpose-built apparatus consisting of an iron support, accessory containers, and an electric gas bubble generator (Figure 3a). The gas bubbles were produced at a stable air flux from the bubble generator and gathered beneath underwater Janus foam. The Janus foam is immersed beneath the water−air interface at a fixed depth of about 2 cm to ensure the flux consistency of the bubble flow. The dynamic process of bubble collection by underwater Janus foam is shown in Figure 3b (also see Movie S2). Zero time was defined as the moment when bubbles initially passed through Janus foam and adhered on the upper surface. Because of the continuous generation of the gas flow from the bottom, the tiny bubble kept growing larger on the upper surface. When the buoyancy force exceeded the adhesion force from the substrate, the gas bubble would detach from the Janus foam and finally be collected. Figure 3c shows the variation of gas/bubble output volume over time (red curve). The blue curve represents the corresponding linear fit result. According to the experimental data, the bubble generator could produce a stable airflow at ~32 mL cm^{-2} min^{-1}. The gas collection rate

https://dx.doi.org/10.1021/acsami.0c00464
ACS Appl. Mater. Interfaces 2020, 12, 18110−18115

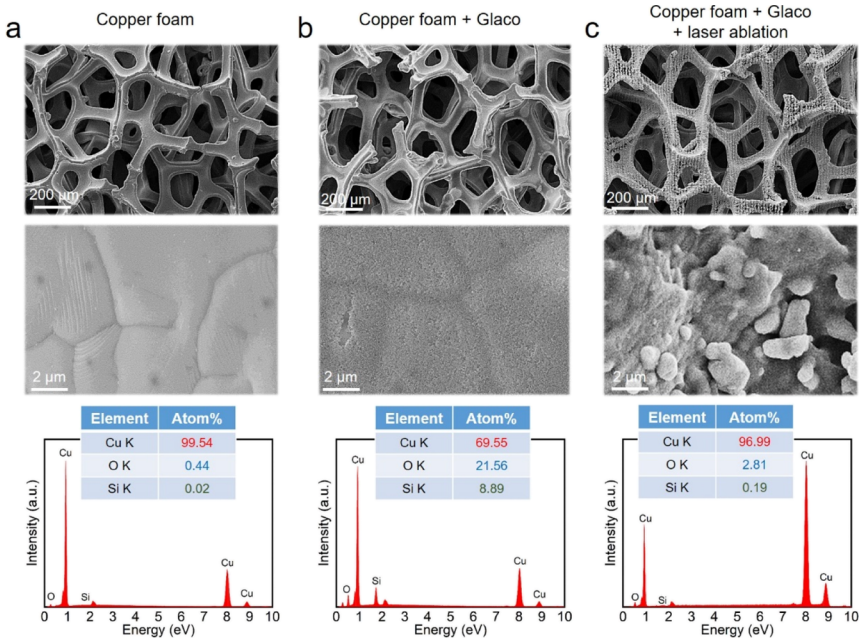

Figure 2. SEM images at different magnifications and EDS element analysis, including Cu, O, and Si for Janus foam in different fabrication stages. (a–c) Pristine copper foam, superhydrophobicity-treated copper foam, and laser-ablated superhydrophobic copper foam.

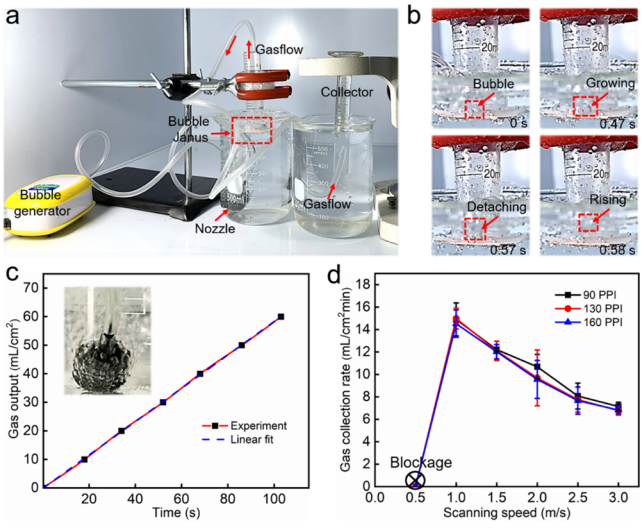

Figure 3. Bubble-collection experiments. (a) Purpose-built apparatus for quantifying bubble collection performance of Janus foam. (b) Dynamic bubble collection process utilizing underwater Janus foam. (c) Gas output stability measurement for the bubble generator device. (d) GCR of Janus foam (90, 130, and 160 PPI) with diverse laser scanning speeds.

(GCR) of Janus foam (90, 130, and 160 PPI) with diverse laser scanning speeds is shown in Figure 3d, from which one can observe that Janus foam exhibited a GCR of approximately 7 mL cm^{-2} min^{-1} at a scanning speed of 3 m s^{-1}. Moreover, the GCR of Janus foam exhibited a maximum value of 15 mL cm^{-2} min^{-1} at a scanning speed of 1 m s^{-1}. In addition, Janus foam showed inconspicuous distinction in GCR among these three PPI values.

Interestingly, it was noticed that when the scanning speed was set to be less than 1 m s^{-1}, Janus foam could hardly collect gas bubbles. This phenomenon is considered to be the fact that a slower laser scanning speed will result in excessive laser ablation, followed by elevated penetration resistance for bubble Janus because of the enlarged thickness of the superhydrophilic (superaerophobic) layer. On the contrary, the GCR of Janus foam gradually decreased with the increase in a laser scanning speed (>1 m s^{-1}), which could be attributed to the reduction of wetting gradient forces between superaerophobic and aerophilic sides. In other words, the superaerophobic surface tends to be aerophobic or even aerophilic as the scanning speed decreases. Noting that the gas collection failure is not equivalent to the gas blockage. As a matter of fact, a membrane with a double-faced fluid affinity (e.g., a double-faced hydrophilic membrane for water droplet) could still transport target fluid slowly in an arbitrary direction.[28] This issue has been studied extensively and goes beyond the scope of this paper. In addition, the GCR exhibited unconspicuous distinction among different samples with 90, 130, and 160 PPI, which demonstrated that the GCR parameter was insensitive to PPI values.

The mechanism of unidirectional bubble penetration through Janus foam was briefly discussed. For Janus foam, the gas bubble only penetrates the foam if the resultant force imposing on the bubble exceeds the resistance from the water film adsorbed in the hydrophilic side of the foam. There are four kinds of forces acting on the water film: the capillary force F_C, gravity force F_G, hysteresis resistance force F_H, and pressure difference F_P between the gas film and the gas bubble (Figure 4a). The capillary force F_C and gravity force F_G are expressed by[16]

$$F_C = 2\pi r\gamma \cos\theta_w \quad (1)$$

$$F_G = \pi r^2 \rho g h \quad (2)$$

where r is the pore radius, γ is the surface tension of water, θ_w is the WCA in air, ρ is the water density, and h is the thickness of the water film. The pressure difference F_P is equal to the gravity force F_G, and the capillary forces F_C from the opposite directions cancel out under a static condition. Generally, the increase in water wettability (as well as WCA θ_w) in the hydrophilic side of the foam would lead to the decline of the F_C along the downward direction. Consequently, the resultant force of two capillary forces would tend to push the bubble upward. It can be deduced that the sole elevation in water wettability is beneficial for the

https://dx.doi.org/10.1021/acsami.0c00464
ACS Appl. Mater. Interfaces 2020, 12, 18110−18115

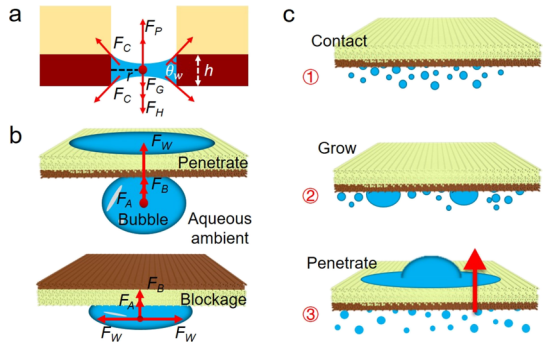

Figure 4. Force analysis regarding (a) water film in a hydrophilic layer and (b) unidirectional bubble penetration through Janus foam. (c) Bubble collection process in different stages, including the initial contact, bubble grow, and penetration.

unidirectional transport and collection performance without modifying the hydrophilic layer thickness. Unfortunately, during the Janus foam fabrication process, the enhancement of laser ablation would also increase the thickness of the hydrophilic layer h, followed by the increase in the gravity force F_G according to eq 2, which is otherwise harmful to bubble penetration. From the Discussion section, it can be found that the construction of both appropriate wettability and thickness of the hydrophilic layer is crucial for spontaneous bubble penetration. However, it is usually difficult in theoretical prediction of the optimum values of water wettability and thickness for the laser-ablated layer. Our exploration suggested that a WCA of ~60° in air, and a laser-ablated-layer thickness of ~100 μm were preferred, and this parametric condition was employed throughout the experiments.

When the gas bubble is attached to the superaerophobic surface (Figure 4b), there are three external forces exerted on the bubble along the penetration direction (upward): the buoyancy force F_B, the wetting gradient force F_W, and the adhesion force F_A. In this case, the resultant force F_R will reach the maximum value

$$F_R = F_B + F_W + F_A \quad (3)$$

With the assistance of the driving force F_R, the enlarged bubble could eventually exceed the external drag forces and thus penetrates Janus foam. Whereas in the contrary direction, the component of the dominant force F_W along the penetrating direction is neutralized. As a consequence, the resultant force $F_R \approx F_B + F_A$ is insufficient to drive the directional movement of gas bubbles. The bubble will horizontally spread on the aerophilic side, resulting in the blockage. The gas collection process includes the initial contact, bubble grow, and final penetration, as shown in Figure 4c. As numerous tiny bubbles contact with the superaerophobic side of Janus foam, the bubbles adhere to the surface and subsequently coalesce into larger bubbles. The enlarged gas bubbles keep growing and penetrating vertically to the aerophilic side when the driving force F_R is large enough. In addition, the internal gas among the foam pores will bridge the gap from the superaerophobic side to the aerophilic side, eventually leading to the spontaneous and continuous transport of gas bubbles in the vertical direction.

Carbon capture and storage are considered to be important and urgently needed in controlling greenhouse gas emissions and their effects on climate change.[35,36] Based on the excellent capability of bubble transport, a demonstrative application of underwater carbon capture utilizing Janus foam was performed. The photograph and schematic of experimental apparatus are shown in Figure 5a and its inset, respectively. A high-purity CO_2 gas flow was continuously generated from a commercial CO_2 generator consisting of a compressed carbon dioxide cylinder and a reducing valve and then passed through the pipe into a water-containing beaker. In order to visualize the chemical reaction process between acidic bubbles and the alkaline solution, a certain amount of the phenolphthalein reagent was added. The reaction between carbon dioxide and sodium hydroxide is described as

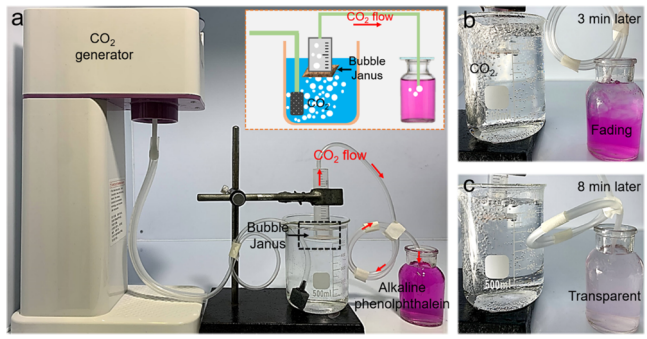

Figure 5. Demonstrative application of the chemical reaction between the CO_2 gas bubble and the alkaline phenolphthalein solution utilizing Janus foam. (a) Experimental setup (inset: schematic of apparatus). (b) Purple solution starts fading after 3 min. (c) Phenolphthalein solution turns transparent after 8 min.

$$NaOH + CO_2 \rightarrow Na_2CO_3 + H_2O$$

As the acidic bubbles were continuously injected into the alkaline solution, the PH value gradually decreased, leading to the decolorization of phenolphthalein. Finally, the color of alkaline phenolphthalein solution was converted from purple-red to transparent after 8 min of the entire reaction (Figure 5b,c and Movie S3). The effective CO_2 capture and transport of this Janus foam could be used in facilitating the sustained harvest of organic gases from the seafloor. It should be emphasized that the gas collection capability of Janus foam is also generic for universal bubble harvest in different gases, which could further broaden its application scenarios.

3. CONCLUSIONS

In conclusion, a kind of Janus copper foam is proposed for unidirectional transport and effective collection of underwater gas bubbles. This Janus foam is fabricated by utilizing a facile and effective ultrafast laser ablation strategy. Janus foam can enable the underwater bubbles to transport spontaneously and unidirectionally from laser-treated side to the untreated side. The underlying physical mechanism of unidirectional penetration is attributed to the cooperation of the buoyancy, adhesion, and wetting gradient forces imposed on the bubble. The gas collection performance of Janus foam prepared with diverse parameters, including the laser scanning speed, and the PPI value is also systematically explored. Our Janus foam exhibits not only the capability of unidirectional penetration of underwater gas bubbles but also the effective gas collection performance with a maximum value of ~15 mL cm^{-2} min^{-1} at a laser scanning speed of 1 m s^{-1}. The proof-of-concept demonstration for underwater carbon capture is shown in which Janus foam could effectively capture underwater CO_2 gas bubbles and facilitate neutralization with the alkaline solution.

https://dx.doi.org/10.1021/acsami.0c00464
ACS Appl. Mater. Interfaces 2020, 12, 18110−18115

We anticipate that the bubble Janus will further extend the applications of bubble transport, carbon capture, and controllable gaseous reactions under aqueous conditions.

4. EXPERIMENTAL SECTION

4.1. Materials and Fabrication. Commercially available copper foam sheets (PPI 90, 130, and 160, thickness ~1 mm) were cut into appropriate sizes and cleaned ultrasonically in acetone and deionized water. The cleaned samples were treated with a commercial coating reagent (Glaco Mirror Coat "Zero", Soft 99 Co.) containing superhydrophobic silica nanoparticles and organic reagents. Thereafter, the superhydrophobic copper foams were mounted on a x-y-z mobile platform and ablated via line-by-line ultrafast laser scanning at different speeds from 0.5 to 3 m/s. The scanning spacing between two adjacent lines was 10 μm in both the x and y coordinates' direction. The laser pulses (a central wavelength of 1064 nm, 150 kHz train of 10 ns) from a nanosecond laser system (JPT, YDFLP-60, Singapore) were focused onto the sample surface and scanned in accordance with the preset pattern through a galvanometric scanning system (SG7110, Sino-Galvo Technology, China) which was equipped with a telecentric f-θ lens with a focal length of 63 mm. The mean power of the laser beam was fixed at ~10 W.

4.2. Characterization. The water/BCAs on Janus foam were measured with a contact-angle system (Innuo CA100C, China) using a sessile drop method. The water/bubble volume was set as 5 μL. Surface morphologies of samples were observed by a secondary electron scanning electron microscope (Zeiss EVO18) with an accelerating voltage at 20 kV. Chemical component analysis was measured through EDS (Bruker XFlash 6130).

4.3. Gas Bubble Collection. The bubble-collecting experiments were carried out on a purpose-built apparatus which consisted of an iron support, accessory containers, and an electric gas bubble generator. The gas bubbles were produced at a stable air flux from the bubble generator and gathered beneath Janus foam which was tightly adhered to the larger end of a plastic syringe. The gas collocation rate of Janus foam was calculated according to the collected volume of gas bubbles versus corresponding elapsed time. Each average value was obtained through five independent experiments at 20 °C temperature and normal atmospheric pressure.

■ ASSOCIATED CONTENT

Supporting Information

The Supporting Information is available free of charge at https://pubs.acs.org/doi/10.1021/acsami.0c00464.

Unidirectional penetration of gas bubbles on Janus foam (AVI)

Bubble penetration process (AVI)

Reaction between CO_2 bubbles and alkaline phenolphthalein (AVI)

■ AUTHOR INFORMATION

Corresponding Authors

Jiawen Li − *CAS Key Laboratory of Mechanical Behavior and Design of Materials, Department of Precision Machinery and Precision Instrumentation, University of Science and Technology of China, Hefei 230026, China;* orcid.org/0000-0003-3950-6212; Email: jwl@ustc.edu.cn

Dong Wu − *CAS Key Laboratory of Mechanical Behavior and Design of Materials, Department of Precision Machinery and Precision Instrumentation, University of Science and Technology of China, Hefei 230026, China;* orcid.org/0000-0003-0623-1515; Email: dongwu@ustc.edu.cn

Authors

Suwan Zhu − *CAS Key Laboratory of Mechanical Behavior and Design of Materials, Department of Precision Machinery and Precision Instrumentation, University of Science and Technology of China, Hefei 230026, China*

Shengwen Cai − *School of Electrical Engineering and Automation, School of Electronics and Information Engineering, Key Laboratory of Computational Intelligence and Signal Processing, Ministry of Education, Anhui University, Hefei 230039, China*

Yucheng Bian − *School of Microelectronics, University of Science and Technology of China, Hefei 230026, P.R. China*

Chao Chen − *CAS Key Laboratory of Mechanical Behavior and Design of Materials, Department of Precision Machinery and Precision Instrumentation, University of Science and Technology of China, Hefei 230026, China*

Bing Xu − *CAS Key Laboratory of Mechanical Behavior and Design of Materials, Department of Precision Machinery and Precision Instrumentation, University of Science and Technology of China, Hefei 230026, China*

Yahui Su − *School of Electrical Engineering and Automation, School of Electronics and Information Engineering, Key Laboratory of Computational Intelligence and Signal Processing, Ministry of Education, Anhui University, Hefei 230039, China*

Yanlei Hu − *CAS Key Laboratory of Mechanical Behavior and Design of Materials, Department of Precision Machinery and Precision Instrumentation, University of Science and Technology of China, Hefei 230026, China;* orcid.org/0000-0003-1964-0043

Jiaru Chu − *CAS Key Laboratory of Mechanical Behavior and Design of Materials, Department of Precision Machinery and Precision Instrumentation, University of Science and Technology of China, Hefei 230026, China;* orcid.org/0000-0001-6472-8103

Complete contact information is available at: https://pubs.acs.org/10.1021/acsami.0c00464

Notes

The authors declare no competing financial interest.

■ ACKNOWLEDGMENTS

This work was supported by the National Natural Science Foundation of China (nos. 51875544, 61505047, and 61805230), the Fundamental Research Funds for the Central Universities (nos. WK2090090025 and JZ2017YYPY0240), the National Key R&D Program of China (2017YFB1104303), the China Postdoctoral Science Foundation (no. 2018M642534). We acknowledge the Experimental Center of Engineering and Material Sciences at USTC for the fabrication and measuring of samples.

■ REFERENCES

(1) Ødegaard, H. The Use of Dissolved Air Flotation in Municipal Wastewater Treatment. *Water Sci. Technol.* **2001**, *43*, 75−81.

(2) Klyavin, O. V.; Likhodedov, N. P.; Orlov, A. N. Dynamic Pipe Diffusion of Impurities through Crystal-gas and Crystal-liquid Interfaces. *Prog. Surf. Sci.* **1990**, *33*, 259−383.

(3) Warnier, M. J. F.; de Croon, M. H. J.; Rebrov, M. E. V.; Schouten, J. C. Pressure Drop of Gas-liquid Taylor Flow in Round Microcapillaries for Low to Intermediate Reynolds Numbers. *Microfluid. Nanofluidics* **2010**, *8*, 33−45.

(4) Sarkar, M. S. K. A.; Donne, S. W.; Evans, G. M. Hydrogen Bubble Flotation of Silica. *Adv. Powder Technol.* **2010**, *21*, 412−418.

(5) Friedlaender, A.; Wiley, D.; Ware, C.; Bocconcelli, A.; Cholewiak, D.; Thompson, M.; Weinrich, M. Underwater Components of Humpback Whale Bubble-net Feeding Behaviour. *Behaviour* **2011**, *148*, 575−602.

(6) Pioro, I. L.; Rohsenow, W.; Doerffer, S. S. Nucleate Pool Boiling Heat Transfer. II: Assessment of Prediction Methods. *Int. J. Heat Mass Tran.* **2004**, *47*, 5045−5057.
(7) Rao, G. V.; Balakrishnan, A. R. Heat Transfer in Nucleate Pool Boiling of Multicomponent Mixtures. *Exp. Therm. Fluid Sci.* **2004**, *29*, 87−103.
(8) Táboas, F.; Vallès, M.; Bourouis, M.; Coronas, A. Pool Boiling of Ammonia/water and Its Pure Components: Comparision of Experimental Data in the Literature with the Predictions of Standard Correlations. *Int. J. Refrig.* **2007**, *30*, 778−788.
(9) Spindler, K. Overview and Discussion on Pool Boiling Heat Transfer Data and Correlations of Ammonia. *Int. J. Refrig.* **2010**, *33*, 1292−1306.
(10) Soloviev, A. V.; Schlüssel, P. Parameterization of the Cool Skin of the Ocean and of the Air-Ocean Gas Transfer on the Basis of Modeling Surface Renewal. *J. Phys. Oceanogr.* **1994**, *24*, 1339−1346.
(11) Pei, C.; Peng, Y.; Zhang, Y.; Tian, D.; Liu, K.; Jiang, L. An Integrated Janus Mesh: Underwater Bubble Antibuoyancy Unidirectional Penetration. *ACS Nano* **2018**, *12*, 5489−5494.
(12) Yu, C.; Cao, M.; Dong, Z.; Wang, J.; Li, K.; Jiang, L. Spontaneous and Directional Transportation of Gas Bubbles on Superhydrophobic Cones. *Adv. Funct. Mater.* **2016**, *26*, 3236−3243.
(13) Yu, C.; Zhang, P.; Wang, J.; Jiang, L. Superwettability of Gas Bubbles and Its Application: From Bioinspiration to Advanced Materials. *Adv. Mater.* **2017**, *29*, 1703053.
(14) Huang, C.; Guo, Z. The Wettability of Gas Bubbles: From Macro Behavior to Nano Structures to Applications. *Nanoscale* **2018**, *10*, 19659−19672.
(15) Duan, J.-A.; Dong, X.; Yin, K.; Yang, S.; Chu, D. A Hierarchical Superaerophilic Cone: Robust Spontaneous and Directional Transport of Gas Bubbles. *Appl. Phys. Lett.* **2018**, *113*, 203704.
(16) Hu, Y.; Qiu, W.; Zhang, Y.; Zhang, Y.; Li, C.; Li, J.; Wu, S.; Zhu, W.; Wu, D.; Chu, J. Channel-Controlled Janus Membrane Fabricated by Simultaneous Laser Ablation and Nanoparticles Deposition for Underwater Bubbles Manipulation. *Appl. Phys. Lett.* **2019**, *114*, 173701.
(17) Lu, Z.; Xu, W.; Ma, J.; Li, Y.; Sun, X.; Jiang, L. Superaerophilic Carbon-Nanotube-Array Electrode for High-Performance Oxygen Reduction Reaction. *Adv. Mater.* **2016**, *28*, 7155−7161.
(18) Zhang, P.; Zhang, J.; Xue, Z.; Wang, J.; Jiang, L. Reliable Manipulation of Gas Bubbles by Regulating Interfacial Morphologies and Chemical Components. *Mater. Horiz.* **2017**, *4*, 665−672.
(19) Yu, C.; Zhu, X.; Cao, M.; Yu, C.; Li, K.; Jiang, L. Superhydrophobic Helix: Controllable and Directional Bubble Transport in an Aqueous Environment. *J. Mater. Chem. A* **2016**, *4*, 16865−16870.
(20) Yin, K.; Yang, S.; Dong, X.; Chu, D.; Gong, X.; Duan, J.-A. Femtosecond Laser Fabrication of Shape-gradient Platform: Underwater Bubbles Continuous Self-driven and Unidirectional Transportation. *Appl. Surf. Sci.* **2019**, *471*, 999−1004.
(21) Yong, J.; Chen, F.; Huo, J.; Fang, Y.; Yang, Q.; Zhang, J.; Hou, X. Femtosecond Laser Induced Underwater Superaerophilic and Superaerophobic PDMS Sheet with Through Microholes for Air Bubbles Selectively Passing Through and Further Collecting Underwater Gas. *Nanoscale* **2018**, *10*, 3688−3696.
(22) Yu, C.; Zhu, X.; Li, K.; Cao, M.; Jiang, L. Manipulating Bubbles in Aqueous Environment via a Lubricant-Infused Slippery Surface. *Adv. Funct. Mater.* **2017**, *27*, 1701605.
(23) Jiao, Y.; Lv, X.; Zhang, Y.; Li, C.; Li, J.; Wu, H.; Xiao, Y.; Wu, S.; Hu, Y.; Wu, D.; Chu, J. Pitcher Plant-bioinspired Bubble Slippery Surface Fabricated by Femtosecond Laser for Buoyancy-driven Bubble Self-transport and Efficient Gas Capture. *Nanoscale* **2019**, *11*, 1370−1378.
(24) Chen, C.; Huang, Z.; Jiao, Y.; Shi, L.-A.; Zhang, Y.; Li, J.; Li, C.; Lv, X.; Wu, S.; Hu, Y.; Zhu, W.; Wu, D.; Chu, J.; Jiang, L. In Situ Reversible Control between Sliding and Pinning for Diverse Liquids under Ultra-Low Voltage. *ACS Nano* **2019**, *13*, 5742−5752.
(25) Zhang, C.; Zhang, B.; Ma, H.; Li, Z.; Xiao, X.; Zhang, Y.; Cui, X.; Yu, C.; Cao, M.; Jiang, L. Bioinspired Pressure-Tolerant Asymmetric Slippery Surface for Continuous Self-Transport of Gas Bubbles in Aqueous Environment. *ACS Nano* **2018**, *12*, 2048−2055.
(26) Xiao, X.; Zhang, C.; Ma, H.; Zhang, Y.; Liu, G.; Cao, M.; Yu, C.; Jiang, L. Bioinspired Slippery Cone for Controllable Manipulation of Gas Bubbles in Low-surface-tension Environment. *ACS Nano* **2019**, *13*, 4083−4090.
(27) Tang, X.; Xiong, H.; Kong, T.; Tian, Y.; Li, W.-D.; Wang, L. Bioinspired Nanostructured Surfaces for On-demand Bubble Transportation. *ACS Appl. Mater. Interfaces* **2018**, *10*, 3029−3038.
(28) Guo, P.; Wang, Z.; Heng, L.; Zhang, Y.; Wang, X.; Jiang, L. Magnetocontrollable Droplet and Bubble Manipulation on a Stable Amphibious Slippery Gel Surface. *Adv. Funct. Mater.* **2019**, *29*, 1808717.
(29) Yang, H.-C.; Hou, J.; Wan, L.-S.; Chen, V.; Xu, Z.-K. Janus Membranes with Asymmetric Wettability for Fine Bubble Aeration. *Adv. Mater. Interfaces* **2016**, *3*, 1500774.
(30) Chen, J.; Liu, Y.; Guo, D.; Cao, M.; Jiang, L. Under-water Unidirectional Air Penetration via a Janus Mesh. *Chem. Commun.* **2015**, *51*, 11872−11875.
(31) Yin, K.; Yang, S.; Dong, X.; Chu, D.; Duan, J.-A.; He, J. Ultrafast Achievement of a Superhydrophilic/Hydrophobic Janus Foam by Femtosecond Laser Ablation for Directional Water Transport and Efficient Fog Harvesting. *ACS Appl. Mater. Interfaces* **2018**, *10*, 31433−31440.
(32) Yang, S.; Yin, K.; Chu, D.; He, J.; Duan, J.-A. Femtosecond Laser Structuring of Janus Foam: Water Spontaneous Antigravity Unidirectional Penetration and Pumping. *Appl. Phys. Lett.* **2018**, *113*, 203701.
(33) Hu, Y.; Wang, Z.; Jin, D.; Zhang, C.; Sun, R.; Li, Z.; Hu, K.; Ni, J.; Cai, Z.; Pan, D.; Wang, X.; Zhu, W.; Li, J.; Wu, D.; Zhang, L.; Chu, J. Botanical-Inspired 4D Printing of Hydrogel at the Microscale. *Adv. Funct. Mater.* **2020**, *30*, 1907377.
(34) Lao, Z.; Zheng, Y.; Dai, Y.; Hu, Y.; Ni, J.; Ji, S.; Cai, Z.; Smith, Z. J.; Li, J.; Zhang, L.; Wu, D.; Chu, J. Nanogap Plasmonic Structures Fabricated by Switchable Capillary-Force Driven Self-Assembly for Localized Sensing of Anticancer Medicines with Microfluidic SERS. *Adv. Funct. Mater.* **2020**, 1909467.
(35) Gibbins, J.; Chalmers, H. Carbon Capture and Storage. *Energy Pol.* **2008**, *36*, 4317−4322.
(36) Scholes, C. A.; Smith, K. H.; Kentish, S. E.; Stevens, G. W. CO_2 Capture from Pre-Combustion Processes-Strategies for Membrane Gas Separation. *Int. J. Greenhouse Gas Control* **2010**, *4*, 739−755.

https://dx.doi.org/10.1021/acsami.0c00464
ACS Appl. Mater. Interfaces 2020, 12, 18110−18115